Science of the Total Environment 885 (2023) 163761

Contents lists available at ScienceDirect

Science of the Total Environment

journal homepage: www.elsevier.com/locate/scitotenv

Multiparametric analysis for the determination of radon potential areas in buildings on different soils of volcanic origin

C. Briones [a], J. Jubera [b], H. Alonso [c], J. Olaiz [b], J.T. Santana [b], N. Rodríguez-Brito [b], A.C. Arriola-Velásquez [c], N. Miquel [c], A. Tejera [c], P. Martel [c], E. González-Díaz [a], J.G. Rubiano [c,*]

[a] Dpto. de Técnicas y Proyectos en Ingeniería y Arquitectura de la Universidad de La Laguna, 38204 Canary Islands, Spain
[b] Servicio de Laboratorios y Calidad de la Construcción del Gobierno de Canarias, 38107 Canary Islands, Spain
[c] Dpto. de Física, Universidad de Las Palmas de Gran Canaria, 35017 Canary Islands, Spain

HIGHLIGHTS

- A methodology to obtain radon risk maps in volcanic islands has been developed.
- Radon risk maps are based on geological criteria and terrestrial gamma radiation.
- Indoor radon data support the goodness of proposed radon risk maps.
- Proxy radiological variables corroborate radon risk maps.
- Current risk areas included in national regulatory maps could be improved.

GRAPHICAL ABSTRACT

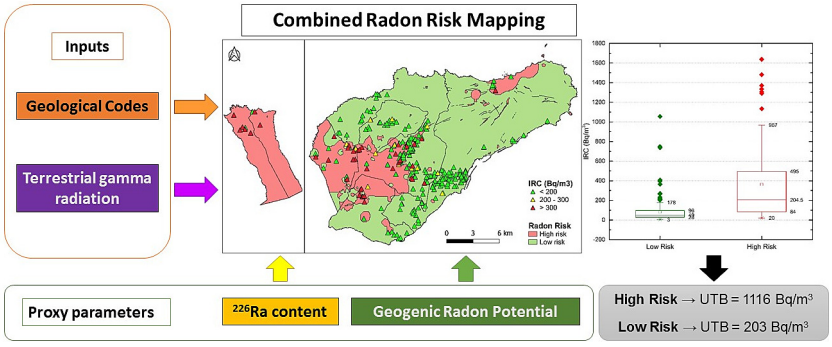

ARTICLE INFO

Editor: Pavlos Kassomenos

Keywords:
Radon
Radioactivity
Gamma radiation
Radioisotopes
Building codes
Risk maps

ABSTRACT

The transposition of the European EURATOM directive into the regulations of the different member states of the European Union involved governments making great efforts to define priority action maps against indoor radon exposure in buildings over a short time period. In Spain, the Technical Building Code established 300 Bq/m^3 as a reference level and set up a classification of municipalities in which remediation measures should be adopted for radon exposure in buildings. Oceanic volcanic islands, such as the Canary Islands, present high geological heterogeneity in a small space due to their volcanic origin. This variability poses a challenge to the elaboration of radiological risk maps, which makes it necessary to have a high density of data to collect local variations. This paper presents a methodology to obtain accurate radon risk maps based on geological criteria and terrestrial gamma radiation. The predictive efficiency of these maps is statistically verified using indoor radon concentration data measured in buildings. Other radiological variables, which are commonly used as criteria for radon risk prediction found in the literature, were also applied, such as the geogenic radon potential and the activity concentration of natural radioisotopes in soils. The higher resolution of the maps obtained allows for a more detailed classification of radon risk zones in the study area than the current risk maps published in the Spanish building regulations.

* Corresponding author.
E-mail address: jesus.garciarubiano@ulpgc.es (J.G. Rubiano).

http://dx.doi.org/10.1016/j.scitotenv.2023.163761
Received 13 February 2023; Received in revised form 2 April 2023; Accepted 23 April 2023
Available online 3 May 2023

1. Introduction

Radon (^{222}Rn) is a colourless, odourless and tasteless radioactive natural gas belonging to the uranium decay chain (^{238}U); it is an element found in the composition of rocks and soils. Approximately 50 % of the radiation to which humans are exposed is due to this gas (UNSCEAR, 2000). The ^{222}Rn generated in rocks and soils in a gaseous state (emanation), is able to reach the atmosphere through pores or fissures in the ground. Outdoors, it would not be a risk to humans because it is found in very low concentrations. However, if this gas accumulates indoors at high concentrations, and humans are exposed to it for prolonged periods, it poses a health risk. Its solid-state progeny, such as ^{218}Po, accumulates in dust particles and can be inhaled and, subsequently, deposited in lung tissue, interacting with it. The World Health Organization (WHO) asserts that, after tobacco, radon is one of the agents that most influences the risk of lung cancer, especially among smokers and ex-smokers (World Health Organization, 2015).

The levels of radon gas concentration that can accumulate in certain rooms within a building depend on natural intrinsic factors as the composition and permeability of soils (Font, 1997), and artificial intrinsic factors as the permeability of the envelopment of the building in contact with the ground and the airtightness of the enclosure envelope (Frutos Vázquez, 2009). In addition, extrinsic factors contribute to radon level variability as meteorological variables, occupancy habits and ventilation regime of the rooms.

Risk maps are extremely important as they assist in providing legislative measures to address priority action areas, implement remediation measures in new buildings and rehabilitate existing housing stock. The geology present in each territory is one of the factors that determine the preparation of these maps. In the case of volcanic islands, such as the Canary Islands, the difficulty involved in the study of this factor acquires certain relevance when considering large geological heterogeneity.

In order to minimise the impact of exposure to high levels of radon concentration on the health of the population, the European Commission published Directive 2013/59/EURATOM of the Basic Safety Standard (BSS) (Euratom, 2014), establishing a maximum reference level of annual indoor radon concentration (IRC) of 300 Bq/m^3. In Spain, this limit of 300 Bq/m^3 was adopted by the transposition of this Directive into the new section HS6 of the basic document DB - HS (Health Standards) of the Technical Code of Buildings (CTE) (Ministerio de Fomento, 2019) and the Royal Decree 1029/2022 of 20 December, approving the Regulation on health protection against the risks arising from exposure to ionizing radiation (Ministerio de la Presidencia, 2022). A classification of radon risk for all the municipalities in Spain was compiled in the Section HS6 of the CTE.

This classification is based on the risk mapping carried out by the Nuclear Safety Council (CSN). In the case of the Canary Islands, the CSN establishes that the islands with the smallest populations are not classified for priority action based on a random variability pattern of IRC values below the reference level (García-Talavera and López-Acevedo, 2019). For the main islands Tenerife and Gran Canaria, which have the largest population, the classification criterion adopted was the chemical composition of the rocks of the different lithostratigraphic units, according to the ratio between the alkaline mineral content (Na2O and K2O) and silicate content (SiO2), using the TAS diagram (R. W. Le Maitre, 2002).

According to this classification, the main islands of the Canary Islands (Tenerife and Gran Canaria), have 50 of their 52 municipalities classified as risk zone, which means that approximately 83.8 % of the population of the Canary Islands live in a radon risk municipality.

The main objective of this paper is to stablish a methodology to obtain accurate radon risk maps based on geological criteria and terrestrial gamma radiation. To achieve this goal, an experimental program was developed that includes several measurement campaigns to determine environmental gamma radiation and indoor radon with a high spatial resolution compared to previous studies. Subsequently, statistical tests have been developed that make it possible to relate with great precision the presence of indoor radon in homes with geology and environmental gamma radiation. To explain the correlations found and reinforce the starting hypothesis, the concentration of ^{226}Ra on the surface and the concentration of radon gas in soils have been used as proxy variables, which have also been determined experimentally in the study area.

2. Materials and methods

2.1. Study area

The study area is made up of 7 municipalities from Tenerife, five of them classified as priority radon risk area (by section HS6 of the basic health document of the CTE), while other two (San Juan de La Rambla and La Guancha) are not classified as risk areas (Ministerio de Fomento, 2019).

In the most populated municipalities, the predominant type of building is a multi-family high-rise residential building. There are also certain areas, especially on the outskirts of both cities, where single-family residential buildings of one or two storeys predominate. In contrast, the study area has an important zone occupying protected natural spaces, where there is very little population settlement (and none at all in certain areas), which makes accessibility difficult. These natural parks are located in the upper reaches of the municipalities of La Guancha and San Juan de La Rambla, and the Anaga Rural Park occupies approximately 145 km^2 in the Metropolitan Area.

2.2. Geological description of the study area

The Canary Islands are an archipelago of volcanic origin, located in the Atlantic Ocean, near to the northwest coast of Africa. It extends for approximately 500 km and is approximately 30 million years old. The volcanic rocks of the archipelago belong to the alkaline igneous series, related to inter-plate volcanism (Carracedo et al., 2002). The most common rocks are basalts (undifferentiated), trachybasalts (intermediate) and phonolites and trachytes (differentiated).

The lithological distribution in the Canary Islands is characterised by a high degree of heterogeneity within relatively small areas, with the consequent complexity of its geological maps. However, different lithologies may have similar values of radiological parameters. A simplified classification of geological codes was made, based on the geochemical characteristics and the radiological behaviour of the set of lithologies that make up volcanic soils. Table 1 shows this classification, which was inspired by the one proposed in (Arnedo et al., 2017) for the Eastern Canary Islands.

According to Arnedo et al., intermediate and acidic rocks (Code A in Table 1) have higher content of ^{226}Ra, ^{232}Th and ^{40}K (particularly ^{226}Ra), respect to basic and ultrabasic rocks (Code B) which exhibit a poor concentration of these radioisotopes. In Table 1, three other geological codes are also established for terrestrial detrital soils, mainly clayey (Code C), terrestrial or marine detrital soils of heterogeneous composition, which we will call deposits (Code D) and lithologies combining rocks belonging to code B and A, which we call mixed rocks (Code M).

In this work, the study area was chosen to cover all the geological codes established for the Canary Islands. A simplified geological map has been

Table 1
Simplified Geological Codes and their most common lithologies.

Code	Description	Most common lithologies
A	Intermediate and acidic rocks	Phonolites, trachytes, trachybasalts, rhyolites, syenites, etc. (and deposits from these rocks)
B	Basic and ultrabasic rocks	Basalts, Basanites, Tephrites, phonolitic tephrites, etc. (and deposits from these rocks)
C	Clay-type terrestrial sediments	Lake soils and sandy-clay soils
D	Deposits	Sands, deposits and debris of generally variable composition depending on the surrounding lithology.
M	Mixed	Lithologies combining igneous rocks of different geological code (A and B).

drawn up (Fig. 1), from 61 different lithologies following the lithostratigraphic map of Canary Islands produced by the Spanish Geological and Mining Institute (I.G.M.E, 2021). Table 2 shows the area covered by each geological code in the study area.

Different geological formations can be distinguished in the study area (Fig. 1). Thus, the Macizo de Anaga Viejo is located in the northeastern part of the island, where basaltic and basaltic-basanitic flows predominate (Code B). Within this massif, we can also distinguish a series of small areas of acidic rocks (Code A), which correspond to phonolitic rocks.

The so-called 'Taganana Arch', located on the north coast, is a large area of deposits formed by alkaline intrusive and extrusive materials, ranging from basalts to phonolites. Its most characteristic unit is a complex of dykes of a salic nature, accompanied by other massive basaltic materials (Hernandez-Pacheco and Rodríguez-Losada, 1996).

The southern and north-western areas of the Metropolitan Area, as well as a large part of Tacoronte, comprise younger geological formations made up of basaltic flows (Code B). The central and western areas of the Metropolitan Area, as well as the south-east of Tacoronte (where there are small differences in elevation), are made up of lacustrine and sandy clay soils (Code C) of different thicknesses.

Finally, the municipalities of La Guancha and San Juan de La Rambla, which are located in the north of the island, are mainly made up of phonolitic flows (in the western half) (Code A) and a group of trachyte, trachybasalt and basaltic flows (in the eastern half) (Code M and B).

Table 2
Number of lithologies and surface area of the study area.

Código	No. of lithologies	Total surface area (km^2)
Acidic (A)	19	29.4
Basic (B)	18	273.9
Clayey (C)	2	25.0
Deposits (D)	9	23.3
Mixed (M)	13	41.6

2.3. Materials

2.3.1. Indoor radon concentration (IRC) measurement equipment

Alpha-track Radosys RSKS detectors, consisting of a diffusion chamber containing a 100 mm^2 CR-39 chip, were used to measure the IRC. Measurement is based on the fact that ^{222}Rn, a radioisotope that is part of the decay chain of ^{238}U, decays into ^{218}Po, resulting in the emission of alpha particles. The typical detector equilibrium time is 3 h and the sensitivity is 2.0 tracks·cm^{2}·-kBq-1·h-1·m^3; saturation limit is >12,000 kBqh/m^3. The typical starting background of the detector is 0.3 tracks·mm^{-2} and its detection limit is 6 Bq/m^3 for 90 days of exposure. Etching was performed using a 25 %/6.25 M sodium-hydroxide solution at an etching temperature of 90 °C, with an etching time of 4.5 h. Two systems were used for processing the dosimeters: NanoBath and NanoReader, and the 2000 System Radometer (by Radosys). This instrumentation is located in the Laboratory and Service of Construction Quality of the Department of Public Works and Transport of the Government of the Canary Islands, on the island of Tenerife, and the Laboratory of Environmental Radioactivity of the Department of Physics of the University of Las Palmas de Gran Canaria, on the island of Gran Canaria. Each detector battery had different calibration parameters, which were supplied by the company and updated by means of the reading software. Periodical comparisons were made between the two laboratories, with external certified laboratories (UCAN) being used to compare the measurements.

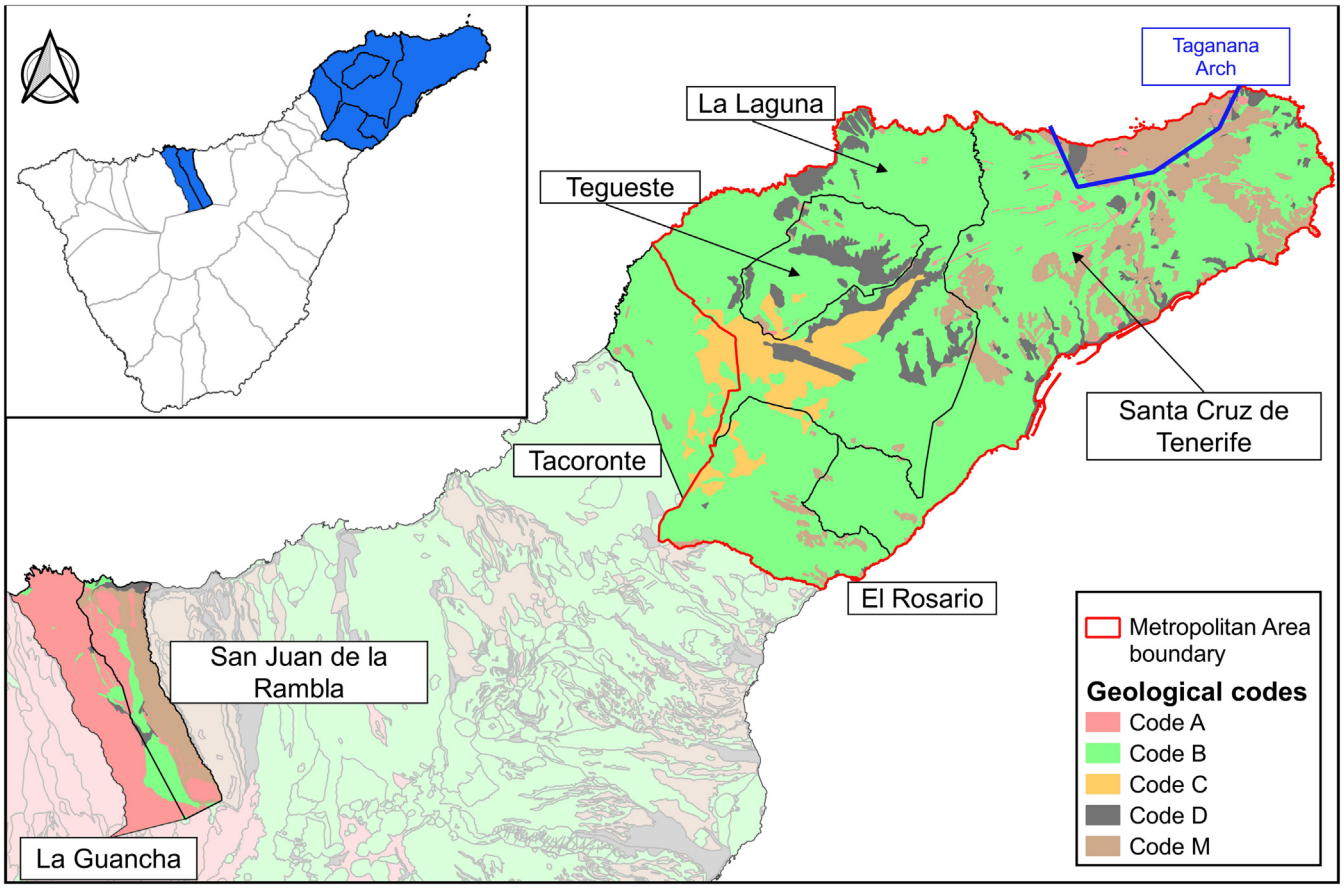

Fig. 1. Municipalities and geological codes in the study area with the delimitation of the Metropolitan area and Taganana Arch.

2.3.2. Gamma radiation measurement equipment

The Ludlum Model 3019 instrument was used to carry out the terrestrial gamma radiation rate measurements, which were then used as a proxy variable to determine areas at risk from high concentrations of IRC. This radiometer model is equipped with an internal Csl scintillation detector with a sensitivity of 175 cpm per μR/h and is used for background measurements of gamma radiation levels up to 500 μSv/h (50μR/h). The radiometer was calibrated in December 2020, prior to the start of the measurement campaign in 2021, by Ludlum Measurements, Inc. The device is transportable and is held on a tripod, to ensure it remains at 1 m above ground level.

2.3.3. Gamma spectrometry equipment

Gamma spectrometry was used as an explanatory variable for the TGR values obtained in the study area. It was performed at the Physics Department of the ULPGC by means of a Canberra Extended Range (XTRa) Germanium spectrometer (model GX3518), with a carbon composite window (0.6 mm thickness), 153 cm^3 active volume and 5 mm length from the detector to the carbon window. The detector has a 38 % relative efficiency, in relation to a NaI(Tl) detector with an active area of 3 × 3″ and nominal FWHMs of 0.875 keV at 122 keV and 1.8 keV at 1.33 MeV. It works when coupled to a DSA-1000 Canberra multichannel analyser. The detector is shielded with 15 cm thick iron and located in a room with walls and a ceiling made of concrete, in the ground floor of a three-floor building. The spectral analysis was performed using the Genie 2000 software package. The relative efficiency calibration of this system was performed using the Canberra LABSOC package, based on the Monte Carlo method. The energy calibration was performed using the 1460.8 keV line of ^{40}K (IAEA pattern: RGK-1 Potassium Sulfate).

The activity concentration of radioisotopes belonging to the ^{238}U and ^{232}Th natural decay chains was determined using the Secular Equilibrium assumption. Thus, the ^{226}Ra activity concentration was obtained from the 351.9 keV gamma emissions from ^{214}Pb, and the activity of ^{232}Th was obtained by means of the 911.2 keV gamma line from ^{228}Ac and 583.2 keV from ^{208}Tl. The activity concentration of ^{40}K was obtained directly from its photopeak of 1460.8 keV. The mean sample counting time was 24 h.

2.3.4. Radon activity concentration in soils and permeability equipment

The GRP is one of the variables commonly used to quantify radon risk. In this work it was used as an alternative variable to validate the risk maps obtained. To carry out the measurement of the radon gas concentrations in soil, the radon v.o.s RM-2 system was used (Neznal et al., 2004). The sampling device was a cylindrical hollow probe of 1 m in length, with an outer diameter of 12 mm and inner diameter of 8 mm. It was equipped with a free, sharpened lower end (a lost tip) of 12 mm diameter.

First of all, at each location, the sharp tip was inserted into the bottom of the probe, which was, in turn, nailed to the respective depth. Then, the tip was pushed down to create a gap in the lower end of the probe, permitting the collection of soil-gas samples, which were drawn up the tube towards the radon measurement equipment.

The soil gas permeability at each point was then obtained using a RADON-JOK permeameter. The principle of this equipment consists of air withdrawal by means of negative pressure. Employing a wire between the probe and the permeameter, the soil gas permeability was calculated using the time taken by the rubber sack in the system to be completely filled with air, with the help of two weights and by employing a nomograph provided by the manufacturer (Radon v.o.s) comprising the relationship between time and permeability.

The methodology for the determination of the activity concentration of radon gas in soil was successfully validated by the participation of three different international comparison measurement exercises of radon in soil gas.

2.4. Methodology

Obtaining reliable risk potential maps using a direct methodology, by measuring the indoor radon activity concentration (Darakctchieva et al., 2015; McColl et al., 2018; J. Miles et al., 2007; J. C. H. Miles et al., 2011), requires a high density of radon measurements for the Canary Islands due to the high lithostratigraphic heterogeneity.

Indirect methods like gamma radiation is widely considered to be a relevant variable for estimating radon risk areas (García-Talavera et al., 2013). On the other hand, the content of ^{226}Ra preceding ^{222}Rn in the radioactive decay series is also related to terrestrial gamma radiation (TGR) and to IRC levels (Arnedo et al., 2017; Briones et al., 2021). Other variables used for estimating radon risk areas are Geogenic Radon Potential (GRP) levels (H. Alonso et al., 2019; Coletti et al., 2022; Pereira et al., 2017) and the radioisotope content of soils and rocks where buildings are located (Ielsch et al., 2010). Therefore, the use of these radiological or geogenic variables, combined with the results obtained by direct measurement (hybrid methods), leads to an improvement in the quality of the RP maps (Cinelli et al., 2011; Fernández et al., 2021; García-Talavera and López-Acevedo, 2019).

2.4.1. Indoor radon concentration (IRC) measurement campaign

In this paper, 277 IRC measurements were made in the study area (Fig. 2), which represents a measurement density of 71 data/100 km^2, appreciably higher than the average density of 10 data/100 km^2 values in Canary Islands currently reported in the literature (García-Talavera and López-Acevedo, 2019; Pinza-Molina, 1998; Robayna Duque, 2002) and considerably greater than the average density of 2.4 data/100 km^2 available for the whole territory of Spain (García-Talavera and López-Acevedo, 2019). The higher density of measurements carried out in this work makes it possible to contemplate the geological heterogeneity of the islands, allowing the improvement of the delimitation of priority action areas.

The experimental campaign of placing radon gas detectors into building enclosures was carried out mainly in residential and single-family buildings. Also, but to a lesser extent, it was measured in dwellings within multi-family apartment buildings and premises.

To minimise the effect of extrinsic factors on the results of the IRC measurements and to homogenise the measurement conditions, a methodology which was defined in previous works was used (Briones et al., 2021). In each building, the measurement was carried out in a representative building enclosure that met the conditions of habitability and which corresponded to the inhabited enclosure of the dwelling. Also, the measurement needed to be located on the floor closest to the ground but above ground level, preferably the ground floor but never above the first floor. Furthermore, the measurement was carried out avoiding the summer months (June to September) and during a minimum period of 3 months.

During the installation process, a protocol was followed to ensure that the dosimeters were not exposed at an inappropriate height, in draughty areas, near heat sources or in uninhabited spaces. Measurements taken in dwellings with an on-ground slab or horizontal air chamber system were not included because they are considered to be dwellings with remediation solutions against the presence of radon gas. All measurements were made with at least two passive detectors measuring in parallel.

2.4.2. Terrestrial gamma radiation (TGR) measurement campaign

With regard to the gamma radiation dose rate, the Map of Natural Gamma Radiation in Spain, drawn up by the Nuclear Safety Council (CSN) and known as MARNA (Suárez-Mahou et al., 2000), includes the gamma radiation measurements for the entire peninsular of Spain. The approximate average density of MARNA is 1.4 data/100 km^2 (Quindós Poncela et al., 2004). However, so far, the Canary Islands have a higher average data density (Table 3).

In this study, the total number of TGR samples in the study area was 302 (Fig. 2). This represents an average density of 76 data/100 km^2 (rising to 111 samples/ 100 km^2 in urban areas), which is 347 % higher than the average density of 17 data/100 km^2 currently available in the literature (Table 3). This density allowed a more precise spatial definition of the radiometric behaviour of the different geologies within each cell and municipality, considering the heterogeneous geological characteristics of oceanic volcanic islands, which is much higher than that of continental territories.

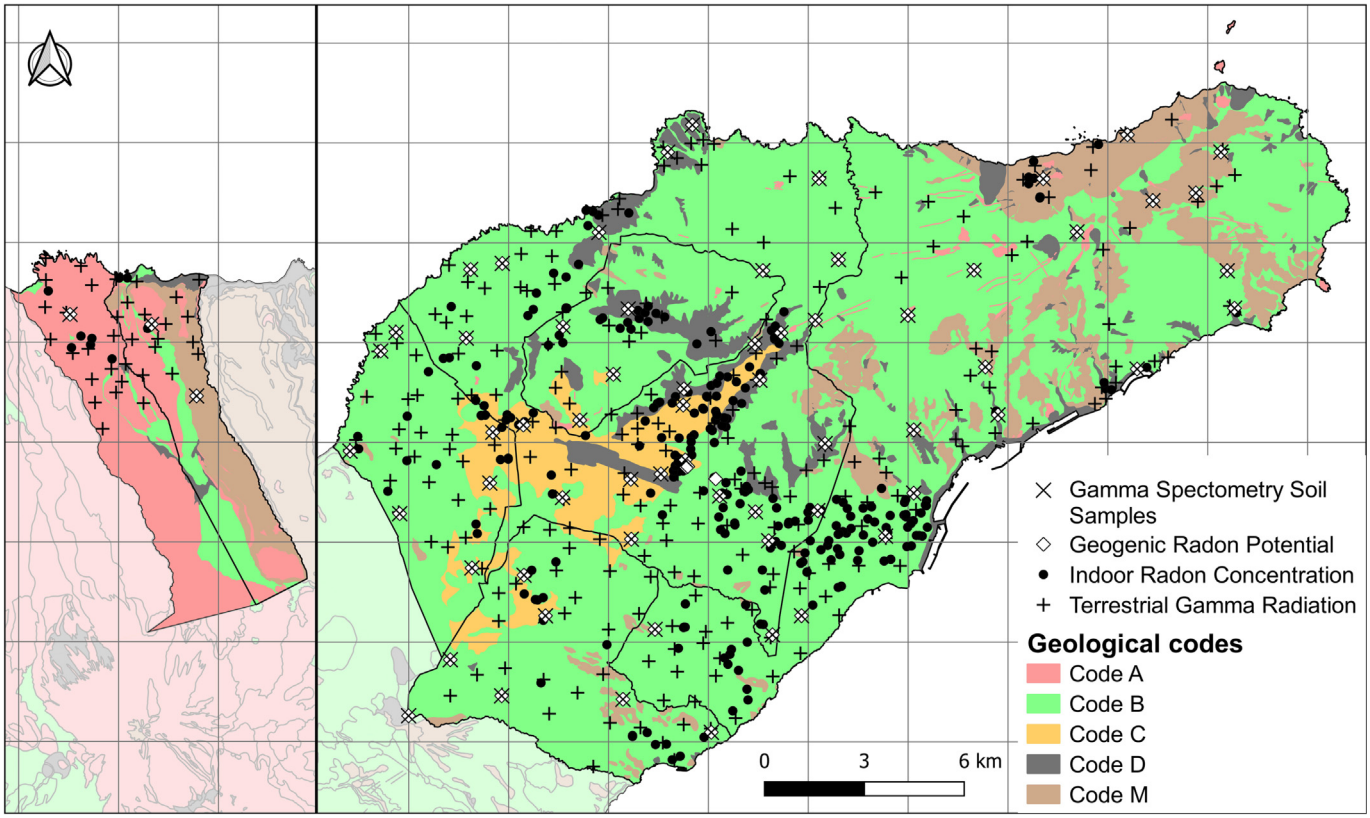

Fig. 2. Location of measurement points of different campaigns on geological codes in the study area.

Taking the correlation between the presence of ^{226}Ra and IRC levels, and its direct influence on TGR dose levels, an intensive TGR measurement campaign was developed in the study area.

For the distribution of the points to be studied in this campaign, a grid of 3 × 3 km was drawn up to cover the entire study area (Fig. 2). The number of points studied per grid was a function of the proportion of urban fabric in each grid so, in areas with a higher percentage of urban fabric, 10 points were carried out and, in those grids located in rural or mountainous areas, 3 points were carried out.

At each location, at least two exposure rate values were taken with the Ludlum 3019 radiometer, placed on a tripod to ensure that it was always 1 m above the ground surface. The two measurements were taken 10 m apart and integrated over 5 min of exposure. If these measurements differed by >10 %, a third measurement was taken at a distance of 10 m from the previous ones, in such a way that the three measurement points formed an approximately equilateral triangle. The final measurement assigned to each point was the arithmetic mean of the measurements taken.

All measurements were taken between 08:00 and 18:00, avoiding measurements on rainy days and leaving a margin of 7 days after the last rainy day, to minimise the influence of soil moisture (Barbosa et al., 2018). Soils that had not been altered by humans (or, at least, as little as possible) were chosen for the measurements. On the other hand, following the criteria established by the CSN (Herranz et al., 2003), flat soils were preferably chosen and the bottoms of ravines were avoided, in the case of measurements on slopes. In addition, nearby obstacles such as trees, dams or reservoirs were avoided, establishing a minimum distance of 15 m from any building and 10 m from walls or paved areas. In built-up urban areas, where compliance with these conditions is complicated, measurements were preferably taken in the central part of accessible plots, as far as possible from any nearby obstacles that could influence the measurements.

Once the measurement campaign was carried out in the study area, the natural gamma radiation dose rate at 1 m from the ground was obtained. In order to obtain the gamma exposure rate exclusively from radioisotopes in the ground (TGR), the cosmic radiation component was disregarded, estimating its value by using the equation considered in the work by Arnedo et al., 2017, for the latitude of the Canary Islands and based on that established in (UNSCEAR, 1993).

2.4.3. Radioisotopic composition measurement campaign

For the concentration of gamma activity of natural radioisotopes in soils, 66 soil samples were taken (Fig. 2), following the Nuclear Safety

Table 3
Available terrestrial gamma radiation (TGR) data in the Canary Islands in the most recent published works.

Reference	Tenerife		Western Islands		Easter Islands	
	Surf.: 2034 km^2		Surf.: 3381 km^2		Surf.: 4066 km^2	
	n	Density (data/100km^2)	n	Density (data/100km^2)	n	Density (data/100km^2)
(López-Pérez et al., 2021)	206	10	352	10	–	–
(Fernández de Aldecoa, 2000)	104	5	133	4	–	–
(Arnedo et al., 2017)	–	–	–	–	600	15
(H. E. Alonso, 2015)	–	–	–	–	176	4
TOTAL	310	15	485	14	776	19

Council's procedure for surface layer sampling (Herranz et al., 2003). For this purpose, surface vegetation was removed at each sampling point, close to the point where the GRP sampling probe was placed. A square of approximately 1 × 1 m was then marked and the sample collected within 5 cm of the topsoil layer.

The samples were crushed in the laboratory and dried in an oven at 80 °C, for 24 h. After drying, the samples were passed through a 1 mm sieve and placed inside PVC containers, up to a volume of 40 cm^3. These containers were sealed with aluminium strips, in order to guarantee tightness and prevent the passage of radon gas, and stored for one month to allow the secular equilibrium between the ^{226}Ra and ^{222}Rn and their short-lived progeny. After this process, the radioisotopes present in the sample were determined by gamma spectrometry.

2.4.4. Geogenic radon potential (GRP) measurement campaign

For this campaign, the sample points were selected and homogeneously distributed on the 3 × 3 km grid with at least one measurement per cell, increasing the density of measurements in the urban area. The radon concentration in soils was measured by introducing the probe to a depth of 80 cm.

Following the methodology established by Neznal et al. (2004), which had already been applied on land in the eastern Canary Islands (H. Alonso et al., 2019), the surface air-tightness of the soil surrounding the probe altered during the driving process, was guaranteed by manual compaction.

2.4.5. Statistical methods

One of the main statistical tools for the identification of radon risk areas used in this work, was the application of calculated statistical tolerance intervals, used according to the method proposed by (García-Talavera et al., 2013) for the development of the indoor radon risk map in Spain. This methodology was also applied in the previous work by Briones et al. (2021), for a case study of radon risk in two representative municipalities in the Canary Islands. Using this methodology, it was possible to obtain the upper tolerance bounds (UTB) of the IRC values of the study area, categorized according to the different variables considered in this work. However, for those categories where the number of available data was not sufficient for the UTB to be an adequate parameter ($n < 27$), other statistical estimators were used, such as the geometric mean and the ninety percentile (P-90), also used in the work by (García-Talavera et al., 2013).

3. Results and discussion

This section first presents the IRC data and its relationship with the different geological codes, from which a risk map based solely on geological criteria is drawn up. Subsequently, in order to explain certain IRC values that are not covered by the first risk map, the relationship of the IRC data with the TGR values obtained by interpolation from a dense measurement campaign was studied, and a risk map based on TGR alone is proposed. Subsequently, a combined map based on geology and TGR is proposed, which allows a more precise delimitation of radon risk areas. Finally, to further analyse the risk areas defined by the combined map, two widely used parameters for the identification of radon risk areas were used: the activity concentration of natural radioisotopes and the GRP.

3.1. Risk map based on IRC measures on geological codes

Geology is one of the main factors influencing radon risk in a given area. In fact, it is one of the most common proxies for radon risk mapping (Cinelli et al., 2011; Hughes et al., 2022; Tondeur and Cinelli, 2014). This section describes the relationship between geological codes and IRC. The spatial distribution of the IRC measurements on the geological map of the study area is shown in Fig. 3a. As can be seen, the measurements are homogeneously distributed in the built-up area, in such a way that the areas with lower density correspond to non-built-up areas.

Fig. 3b shows a box-and-whisker plot of the IRC values grouped by geological codes. There are no differences between the IRC values associated with codes B, D and M, or between codes A and C. However, there are statistically significant differences between the IRC measurements included in codes B, D and M and those corresponding to codes A and C. This means that the IRC values are lower for dwellings on basic rocks and deposits and mixed rocks than the IRC values obtained for dwellings on acidic rocks and clays. Thus, in the case of basic rocks (Code B), the indicators of the statistical analysis in Table 4 show low values in relation to radon risk (Xg = 53.5 Bq/m^3, UTB = 255 Bq/m^3, P-90 = 208 Bq/m^3) and similar results are obtained in codes M and D. Therefore, the areas in which these codes appear could reasonably be classified as Non-Prone radon areas.

Analysing these values, it is observed that the UTB of the IRC values associated with code C is higher than the reference level of 300 Bq/m^3. In the case of code A, there is insufficient data available for the calculation of UTB but both GM and P-90 exceed the indicative value of 300 Bq/m^3. A risk map based on these results is shown in Fig. 4a, where the areas corresponding to codes A and C are classified as high radon risk areas, while codes B, D, and M are classified as low risk areas (García-Talavera and López-Acevedo, 2019). As shown in Fig. 4b, regarding the total IRC data measured in the study area, the high-risk area collects 68 % of the data above 300 Bq/m^3, while the remaining 32 % is in the low-risk area. This implies that, in the area classified as risky, 52 % of the measured IRC data exceed the reference level of 300 Bq/m^3 while, in the area considered as being low-risk, only 5.8 % of the data exceed the reference level.

The risk map in Fig. 4 identifies those municipalities with a larger area in codes A or C as higher risk. To illustrate this result, Table 5 shows the percentage of area occupied by the different codes for each municipality. Thus, the municipalities of La Guancha with 97 % of its surface in code A would present a high risk of radon. In contrast, Santa Cruz de Tenerife, with almost 92 % of its area in code B, could be classified as a low risk area for radon. In these two most extreme cases, the IRC data agree very closely with this assumption.

3.2. Risk map based on terrestrial gamma radiation (TGR) measurements

A total of 302 TGR measurements were carried out for the study area, homogeneously distributed in the different geological codes (Fig. 2).

In this work, the establishment of radon risk maps taking TGR as the decision parameter was based on the gamma radiation intervals proposed by the CSN (García-Talavera and López-Acevedo, 2019) to classify priority action areas due to radon exposure, which is expressed in terms of geometric mean (Table 6). García-Talavera established that a TGR level of 7.5 μR/h is a reliable indicator that a given area should be treated as a priority action zone (García-Talavera and López-Acevedo, 2019).

Following this criterion, Table 7 shows that the measurements taken on the majority of the geology of the islands consisting of basic rocks (Code B), show a geometric mean of 5.3 μR/h, which corresponds to a low potential exposure. However, clayey soils (Code C) have a higher geometric mean of 8.6 μR/h, which is a medium potential exposure (Table 6). Higher values are found in the averages for acidic soils (Code A). These soils are mainly formed by phonolites and have a geometric mean higher than 14 μR/h (Table 7), in the high potential exposure range.

To relate the TGR data to the IRC values measured, an inverse distance weighted interpolation (IDW) of the TGR results in the study area was then performed (Fig. 5a). This interpolation makes it possible to determine the TGR value corresponding to the location of each of the points at which the IRC was measured.

Fig. 5b shows a box-and-plot diagram with the IRC results distributed according to the TGR ranges established by the CSN (Table 6). The differences between the different groups are quantified by determining the UTB of IRC values for the three gamma radiation sections, according to the limits described (Table 8). As can be seen, the areas with the lowest gamma radiation (< 7.5 μR/h) show a UTB below the reference level of 300 Bq/m^3, corresponding to an area covering 76.2 % of the buildings analysed. Areas with a TGR between 7.5 μR/h and 14 μR/h, have a UTB

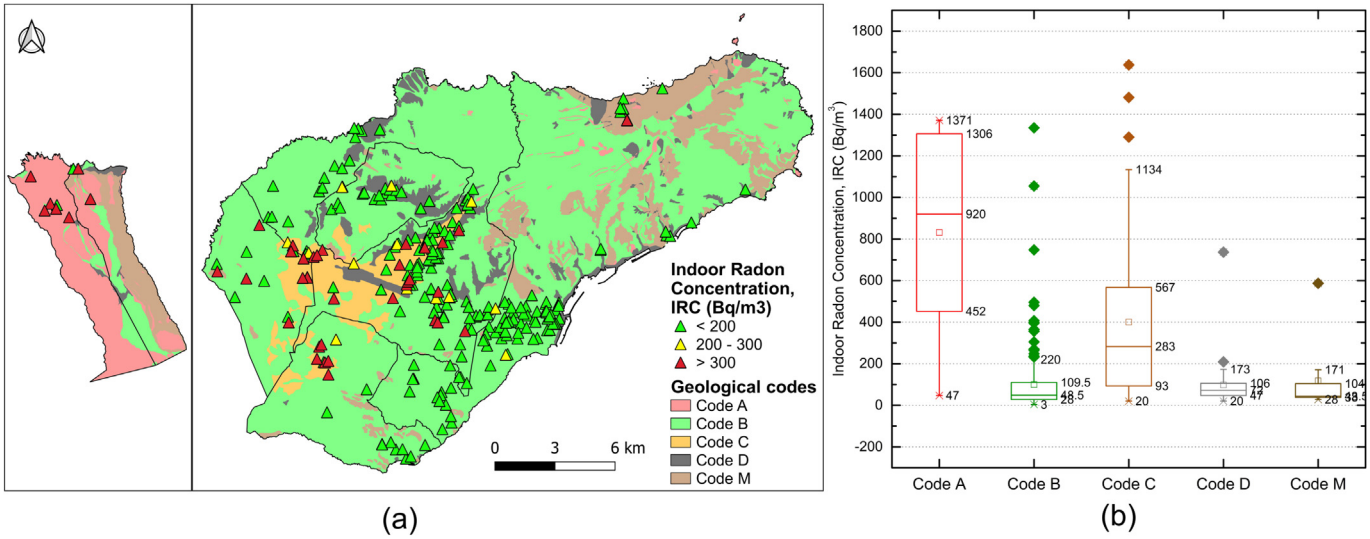

Fig. 3. Indoor radon concentration (IRC) values on geological code map (a) and box-and-whisker plot of IRC results categorized by geological code (b).

Table 4
Statistical comparison of indoor radon concentration (IRC) results categorized by geological code.

	Code A	Code B	Code C	Code D	Code M
n	7	176	47	37	10
GM (Bq/m^3)	592.4	53.5	240.7	73.7	68.4
GSD (Bq/m^3)	3.2	3.0	3.0	2.0	2.6
UTB (Bq/m^3)	([a])	255	1325	222	([a])
P-90 (Bq/m^3)	1332	208	877	146	213

[a] Non-significant value due to low number of samples.

of 1074 Bq/m^3, higher than the reference level, and for areas with a TGR higher than 14 μR/h, the UTB value is not statistically representative because it is clearly influenced by the low number of samples. However, the geometric mean (above the reference level) is 750 % higher than the group of IRC values in the low TGR range, and the P-90 of these values is 531 % higher.

Fig. 6a shows a radon risk map based on the TGR results, where areas obtained by interpolation above 7.5 μR/h are classified as high-risk areas and areas with a TGR below this value are classified as low-risk areas (García-Talavera and López-Acevedo, 2019). This map also shows the IRC data, which allows us to verify its predictive capacity. As shown in Fig. 6b, regarding the total IRC data measured in the study area, the high-risk area collects 66 % of the results above 300 Bq/m^3, while the remaining 34 % are in the low-risk area. This implies that 42 % of the measured IRC data in high-risk areas exceed the reference level of 300 Bq/m^3, while only 7 % of the IRC data in low-risk areas exceed this reference level.

3.3. Combined risk map: geology and terrestrial gamma radiation (TGR)

Fig. 6a shows that the risk map based on TGR is able to explain the high IRC values in the northwest area (municipality of Tacoronte). On the geological map, this area belongs to Code B but the TGR measurement allows us to differentiate its radiological behaviour from other basaltic areas. In this way, the availability of a map with a high resolution of TGR allows us to refine radiological risk maps based on geological criteria, which have experimental and cartographic uncertainties. Therefore, a second approximation to the radon risk map in the study area is obtained by combining the geology-based risk map with the TGR-based one. This map is shown in Fig. 7a.

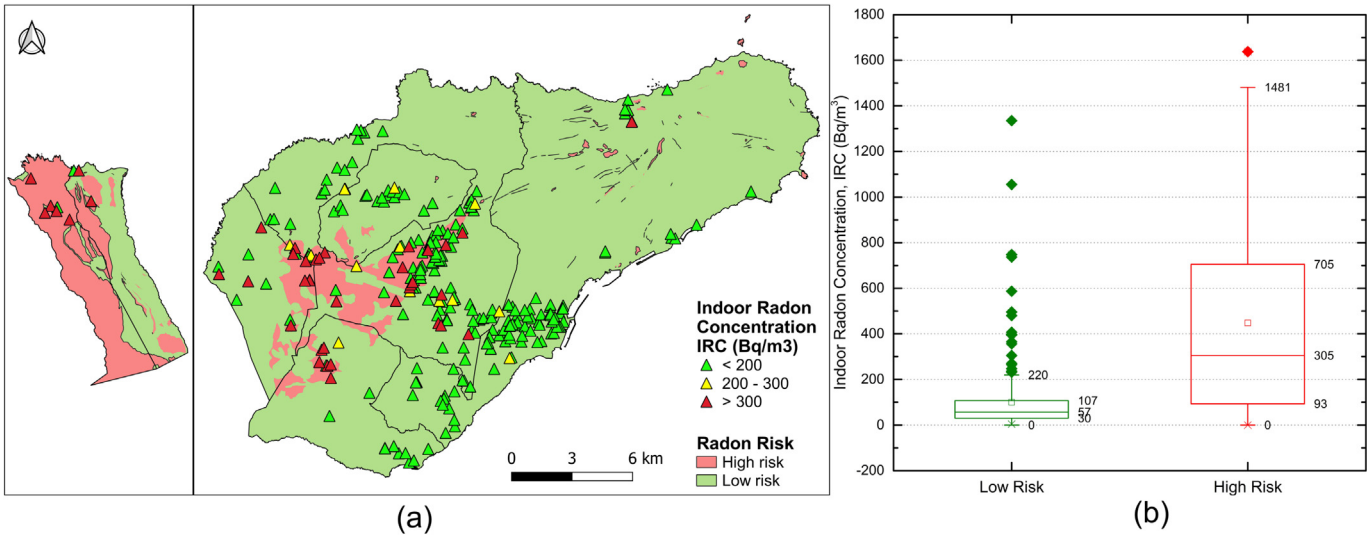

Fig. 4. Indoor radon concentration (IRC) values on radon risk map based on geology alone (a) and box-and-whisker plot of IRC results categorized by radon risk (b).

Table 5
Geographical and geological characteristics of the municipalities in the study area.

Municipality	Surface (km^2)	Pop. (inh.)	Density (inh./km^2)	Urban fabric (km^2)	% of geological code on urban fabric				
					A	B	C	D	M
Santa Cruz de Tenerife	150.6	208,563	1385.3	18.9	0.2	91.6	0.0	2.4	5.9
La Laguna	102.1	158,010	1548.2	30.8	0.0	65.2	24.6	10.0	0.3
El Rosario	39.4	17,590	446.1	8.1	0.0	84.1	11.1	0.3	4.6
Tegueste	26.4	11,326	428.9	5.0	0.5	53.9	10.1	34.6	0.6
Tacoronte	30.1	24,346	809.1	10.3	0.0	79.8	19.1	0.0	1.1
San Juan de La Rambla	20.7	4,854	235.0	1.8	49.0	25.5	0.0	7.6	17.9
La Guancha	23.8	5,553	233.5	1.7	97.0	2.1	0.0	1.0	0.0
Total Study Area	393.0	430,242	1094.8	76.6	3.4	72.6	14.3	7.1	2.7

Table 6
Gamma radiation intervals and corresponding radon exposure expressed in terms of geometric mean (GM) (García-Talavera and López-Acevedo, 2019).

Potential exposure	Gamma exposure rate (μR/h)	Radon exposure (GM)
Low	< 7.5	< 70 Bq/m^3
Medium	7.5–14.0	70–120 Bq/m^3
High	> 14.0	> 120 Bq/m^3

Table 7
Statistical comparison of terrestrial gamma radiation (TGR) results categorized by geological code.

	Code A	Code B	Code C	Code D	Code M
n	29	185	32	25	31
AM (μR/h)	19.2	5.9	8.8	5.9	7.6
SD (μR/h)	6.2	2.6	1.8	2.5	3.2
GM (μR/h)	18.1	5.3	8.6	4.6	7.0
GSD (μR/h)	3.7	1.7	1.7	3.7	1.7

The combined risk map shows 85 % of the IRC values above 300 Bq/m^3 in the risk area, which represents 41 % of the total IRC values in this area (Fig. 7b and c). By contrast, in the low-risk zone, 97 % of the IRC data are below the reference level of 300 Bq/m^3. If we calculate the UTB for each zone, we obtain a value of 1116 Bq/m^3 for the zone considered to be at risk, compared to 203 Bq/m^3 for the low-risk zone. These results show that a combined Geology – TGR risk map is useful for the delimitation of radon risk areas.

Table 8
Indoor radon concentration (IRC) results by terrestrial gamma radiation (TGR) level.

	TGR < 7.5 μR/h	7.5 < TGR < 14 μR/h	TGR > 14 μR/h
n	212	56	9
GM (Bq/m^3)	57.3	178.0	487.3
GSD (Bq/m^3)	2.9	3.2	3.1
UTB (Bq/m^3)	256	1074	([a])
P-90 (Bq/m^3)	209	829	1319

[a] Non-significant value due to low number of samples.

The predictive power of the combined map respect to those based solely on TGR or geology can be clearly seen by analysing the UTB values in the high and low risk zones defined in the different maps. Thus, the UTB of the IRC data in the low risk zone are 245 Bq/m^3 (Geology), 256 Bq/m^3 (TGR) and 203 Bq/m^3 (Combined). As can be seen, the combined map defines a low risk zone that allows a greater safety margin in relation to the reference level 300 Bq/m^3. This would even allow this combined risk map to be maintained in the event of possible decreases in the reference limit from 300 Bq/m^3 to 200 Bq/m^3. In fact, the number of high data respect to the amount of data in the low risk zone of the combined map is only 3 % compared to 6 % for the geology-based map or 7 % for the TGR-based map. Therefore, the combined map allows us to more clearly define a low risk zone. On the other hand, in the high – risk zone, the UTBs provided by the three maps exceed 1000 Bq/m3 (clearly above the reference level), but the combined risk map collects 85 % of the data over 300 Bq/m^3 measured in the study area compared to 68 % of the geology-based map or 66 % of the TGR-based map.

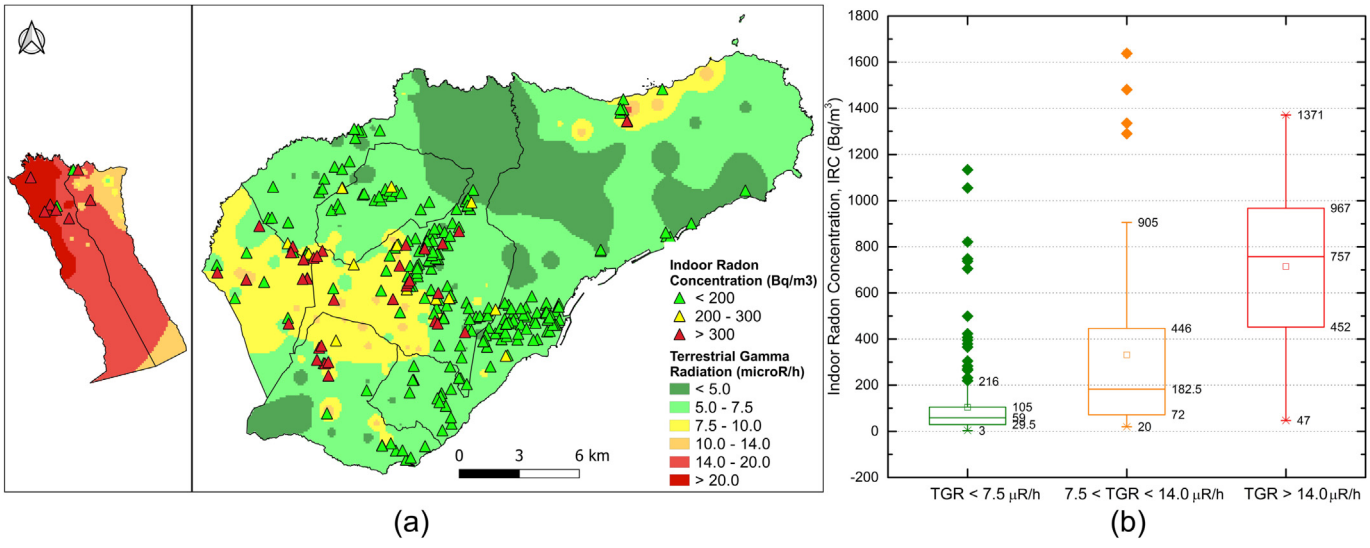

Fig. 5. Indoor radon concentratioon (IRC) values on terrestrial gamma radiation (TGR) interpolation map (a) and box-and-whisker plot of IRC categorized by TGR range (b).

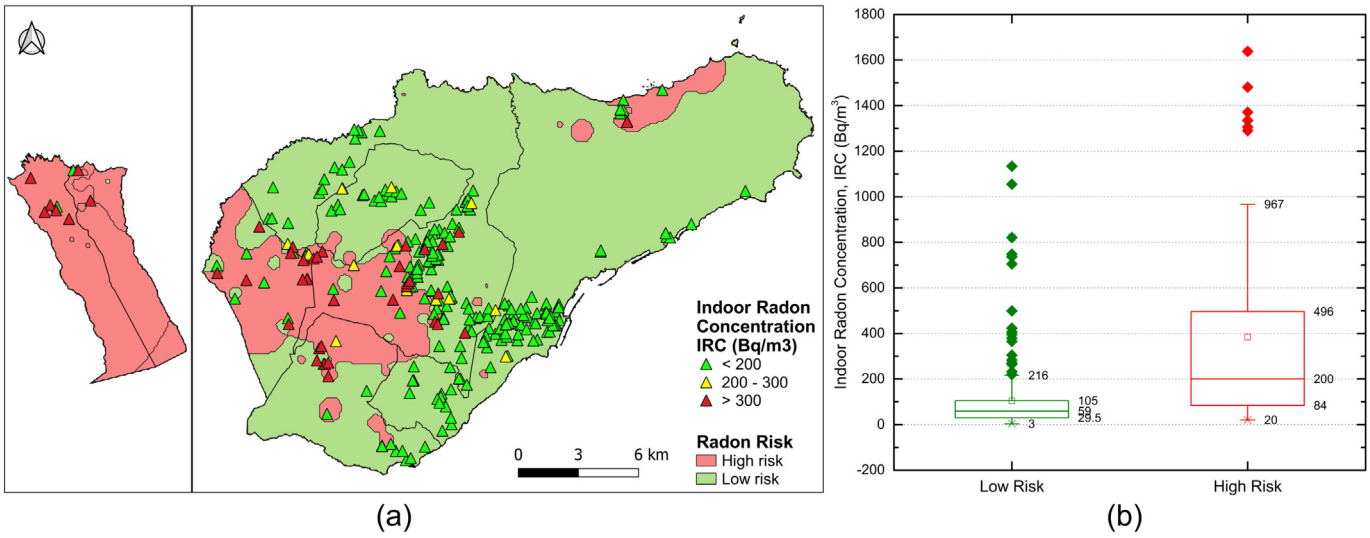

Fig. 6. Indoor radon concentration (IRC) values on risk map based on terrestrial gamma radiation (TGR) alone (a) and box-and-whisker plot of IRC results categorized by radon risk (b).

3.4. Validation of the combined geology – TGR risk map from measurements of environmental radiological variables

3.4.1. Natural radioisotope activity concentration

To validate the combined risk map, the radioisotopic activity concentration of soil was used. For this purpose, 66 soil samples were collected and homogeneously distributed in the study area, to determine the activity concentration of the natural radioisotopes (^{226}Ra, ^{228}Ra, and ^{40}K) by means of high-resolution gamma spectrometry. Since ^{226}Ra is the parent radioisotope of ^{222}Rn, the activity concentration of ^{226}Ra is expected to have a good spatial correlation with IRC levels in the study area.

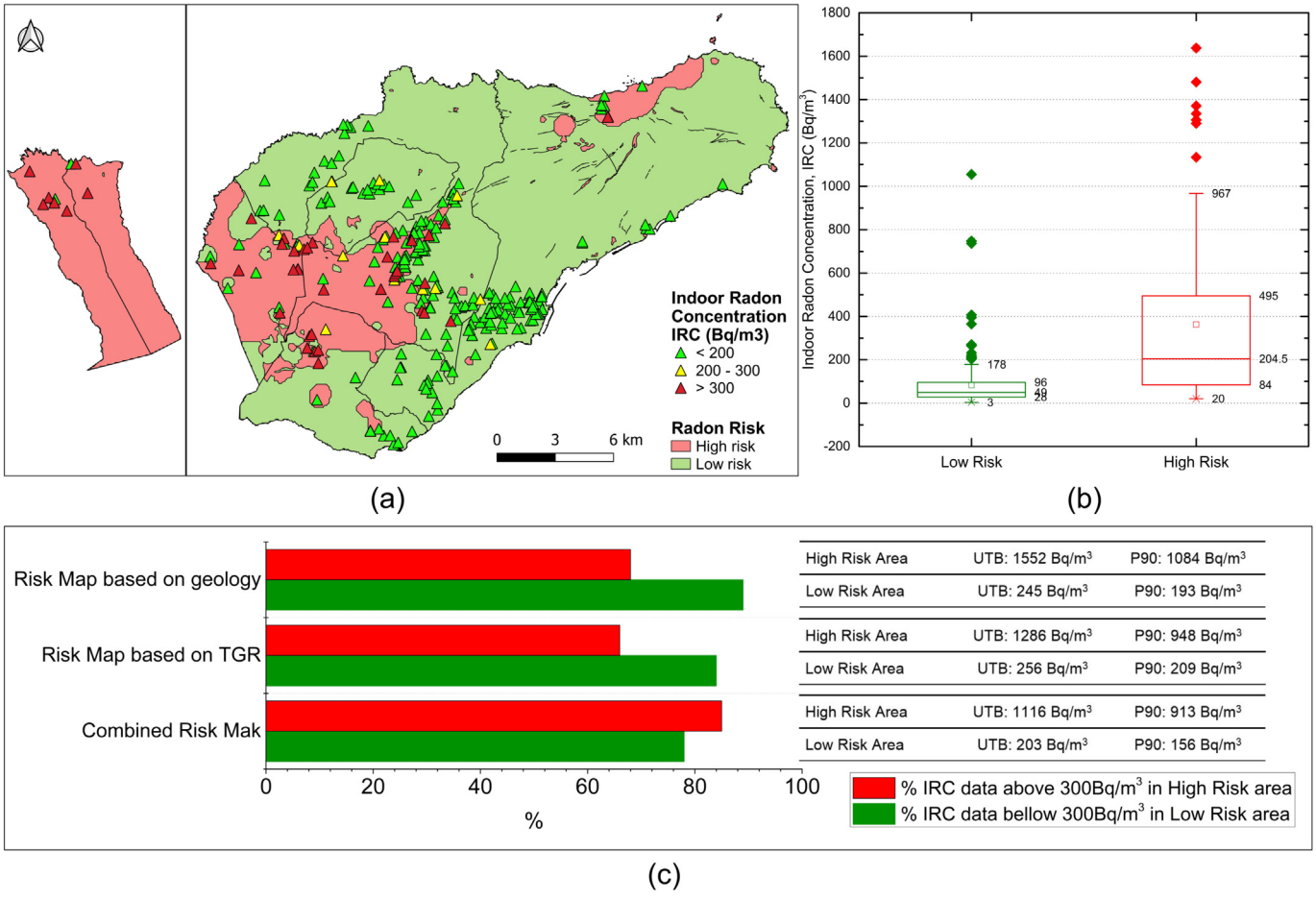

Fig. 7. Combined radon risk map of the study area based on geology and terrestrial gamma radiation, TGR (a), box-and-whisker plot of indoor radon concentration (IRC) results categorized by radon risk (b) and percentages of IRC data in radon risk areas and statistical results of different risk maps.

This was demonstrated by the IDW interpolation maps of the study area, made using the activity concentration values of ^{226}Ra (Fig. 8a), ^{228}Ra (Fig. 8b), and ^{40}K (Fig. 8c).

Table 9 shows the UTB and P-90 calculations of the IRC values as a function of the ^{226}Ra activity concentration. To perform the calculations shown, each IRC value was associated with its value of ^{226}Ra, corresponding to its location obtained by interpolation of the map in Fig. 7a. To establish the high, medium and low categories, a lower limit of 27 Bq/kg of ^{226}Ra concentration was chosen and the UTB of the IRC associated with this value was <200 Bq/m^3. The upper limit of ^{226}Ra chosen (45 Bq/kg) corresponds to a UTB above 300 Bq/m^3 (reference level).

If the interpolation map of ^{228}Ra concentration values (Fig. 8b) is analysed, areas of high activity concentration are identified, similar to the case of ^{226}Ra. In this case, the GM of the ^{228}Ra concentration values obtained in soils of code C is 55 % higher than the GM of the samples in code B. However, the interpolation map of the ^{40}K activity concentration values does not allow the prediction of radon-prone areas, with no significant differences between the different geological codes (Fig. 8c).

In order to check this, from the activity concentration values of these three natural radioisotopes, analysed in each sample, it is possible to estimate the gamma radiation dose rate in nGy/h in outdoor air at 1 m from the ground, using Eq. (1) (UNSCEAR, 2000):

$$D\ (nGy/h) = 0.462 \times C_{Ra\ -\ 226} + 0.604 \times C_{Th\ -\ 232} + 0.0417 \times C_{K\ -\ 40} \quad (1)$$

In this equation, the conversion factors multiplying $C_{Ra\text{-}226}$, $C_{Th\text{-}232}$ and $C_{K\text{-}40}$ were used to convert the activity concentration of ^{226}Ra, ^{228}Ra and ^{40}K, respectively, as proposed in (UNSCEAR, 2000). Fig. 8d shows the IDW interpolation of the estimated gamma dose rate values, in μR/h, from the radioisotope content of the soils in the study area over which the experimental TGR values are shown and by applying the intervals already described above. In this figure, it can be seen that the experimental TGR values are in accordance with the estimations. Thus, 86 % of the TGR values measured in areas with an estimated TGR lower than 7.5 μR/h, are also below this level. On the other hand, in areas with an estimated TGR higher than 7.5 μR/h, 82 % of the measured TGR values are also above this limit.

Table 9
Statistical comparison of indoor radon concentration (IRC) results categorized by level of ^{226}Ra activity concentration. (Bq/kg).

	^{226}Ra < 27 Bq/kg	27 < ^{226}Ra < 45 Bq/kg	^{226}Ra > 45 Bq/kg
n	44	191	42
GM (Bq/m^3)	31.3	70.8	296.4
GSD (Bq/m^3)	2.9	2.7	3.2
UTB (Bq/m^3)	171	295	1901
P-90 (Bq/m^3)	110	270	1304

Fig. 9a shows the combined Geology - TGR risk map on which the activity concentration results of ^{226}Ra are coloured, according to the ranges described. It can be seen that 94 % of the ^{226}Ra concentration values above 45 Bq/kg are within the high–risk area. This implies differentiated behaviour in the two risk zones (Fig. 9b), with a GM of the ^{226}Ra values of 43.4 Bq/kg in the high–risk area, being 91 % higher than the GM of the ^{226}Ra values in the low radon risk area (22.7 Bq/kg).

The concentration of ^{226}Ra also makes it possible to differentiate the basaltic area of the municipality of Tacoronte from other areas with the same geology, in a similar way to the TGR. This corroborates the good fit of using the combined risk map.

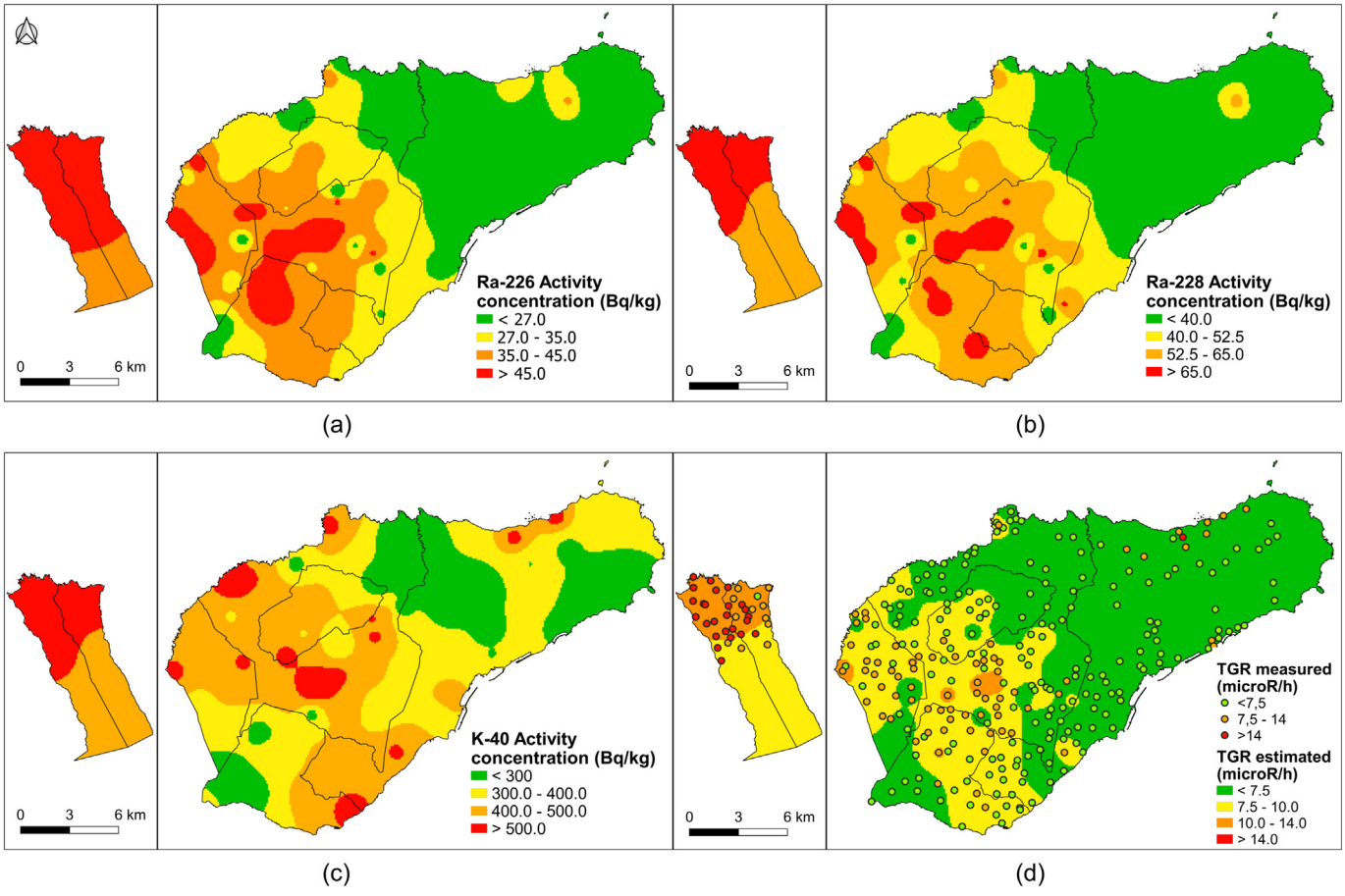

Fig. 8. IDW interpolation map of ^{226}Ra activity concentration (a), ^{228}Ra activity concentration (b) and ^{40}K (c) activity concentration; and experimentally measured terrestrial gamma radiation (TGR) values on TGR interpolation map estimated from natural radioisotope activity concentration in soil (d).

3.4.2. Geogenic radon potential (GRP)

Other variables for radon risk identification are GRP from the radon activity concentration in soil and permeability. To compare its predictive capacity, 69 GRP measurements were carried out in the study area. Fig. 2 shows the locations where GRP samples were taken on the simplified geological code map. To determine the GRP value, we used the definition made by Neznal (Neznal et al., 2004), calculated by the following heuristic equation (Eq. (2)):

$$GRP = \left(\frac{C_{Rn}}{-\log_{10}(k) - 10}\right) \quad (2)$$

where C_{Rn} is the radon concentration in soil (kBq/m^3) and k is the permeability in m^{-2}.

This approximation can be graphically represented by plotting the log of the permeability on the y-axis and the radon concentration on the x-axis (Neznal et al., 2004). Fig. 10 shows this graphical representation, in which the boundaries between high, medium and low GRP zones are plotted; the symbology of the values is arranged according to the geological code. The radon gas concentration in soils shows a wide variability, which is in accordance with the geological heterogeneity of the study area. However, it can be distinguished that high GRP values are mainly concentrated in areas with clay soils (Code C). In contrast, medium and low GRP values are mainly located in basic soils (Code B), mixed soils (Code M) and deposits (Code D).

An IDW interpolation map of the GRP measurements was made in the study area. Fig. 11a shows the IRC results on the GRP interpolation map. It can be seen that the points with the highest IRC values are located in areas of medium to high GRP, so areas with GRP < 10 host IRC values below 200 Bq/m^3.

From the IDW interpolation of the GRP measurements, the values corresponding to the location where the IRC measurements were taken have been extracted and the pairs of values were grouped into three categories of GRP level. A differentiated behaviour of these ranges can be seen in the box-and-whisker plot in Fig. 11b.

To verify the difference in these three groups, the calculation of tolerance limits was applied. Table 10 shows that the IRC measurements taken in areas with low GRP have a UTB of 241 Bq/m^3 (lower than the reference level), while the measurements taken in areas with high GRP (above 35) have a UTB of 2505 Bq/m^3, 735 % higher than the reference level. In the case of IRC measurements located in medium GRP areas (which account for 77 % of all IRC measurements), they have a UTB of 330 Bq/m^3, only 10 % higher than the reference level (300 Bq/m^3).

Fig. 12a shows the combined geology and TGR risk map on which the GRP results are coloured according to the ranges already defined. In this case, it can be seen that 88 % of the GRP values above 35 are within the high–risk area, while 77 % of the GRP values below 10 are outside this area. Fig. 12b shows that the GRP values in the high–risk area have a GM of 16.8, 115 % higher than the GM obtained from the GRP values in the low–risk area. These results are also in accordance with the risk zones established in the combined Geology – TGR risk map.

4. Conclusions

This work has developed a methodology for the estimation of indoor radon risk based on the combination of geology and terrestrial gamma radiation in volcanic terrain, characterised by its high lithostratigraphic heterogeneity.

1) In terms of geology, the different lithologies typical of oceanic volcanic islands, such as the Canary Islands, were simplified into five geological codes based on their composition and radiological behaviour. The study area of this work includes all types of geological codes, with Code B being the most abundant type and Code A soils being concentrated mainly in the municipalities of La Guancha and San Juan de la Rambla; Code C soils were predominant in the central part of the Metropolitan Area (La Laguna, Tacoronte and El Rosario). A close correlation was found between acidic (A) and clayey (C) geological codes and high indoor radon concentrations.
2) However, the risk map based exclusively on geological criteria does not explain all the high IRC values found. A profuse campaign of TGR measurements in the study area has facilitated the elaboration of a more precise map that allows extending the risk zone obtained from the geology by including certain basaltic areas (Code B) with high TGR values. In other words, the combined risk map obtained is better adapted to the experimental IRC data measured in the study area. In this sense, the areas classified as high-risk on this map have 85 % of the IRC results above the reference level (300 Bq/m^3), obtaining a UTB of IRC values of 1116 Bq/m^3. In contrast, the areas classified as low–risk have a UTB of 203 Bq/m^3, as 97 % of the IRC values measured in this area are below the reference level.
3) This widening of the risk areas based on TGR can also be explained by the measurement of other radiological variables, such as the activity concentration of ^{226}Ra and the geogenic radon potential (GRP). In this sense, 94 % of the ^{226}Ra concentration values above 45 Bq/kg were collected in high-risk areas of the combined risk map. This makes the

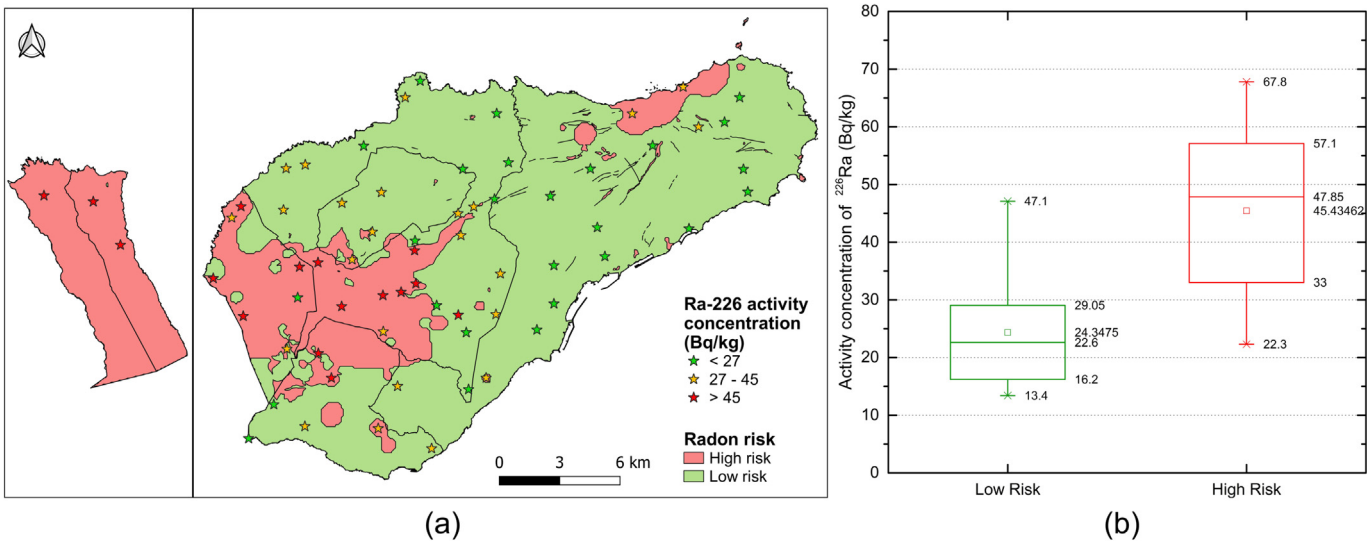

Fig. 9. ^{226}Ra activity concentration values on combined radon risk map (a), box-and-whisker plot of ^{226}Ra values categorized by radon risk level (b).

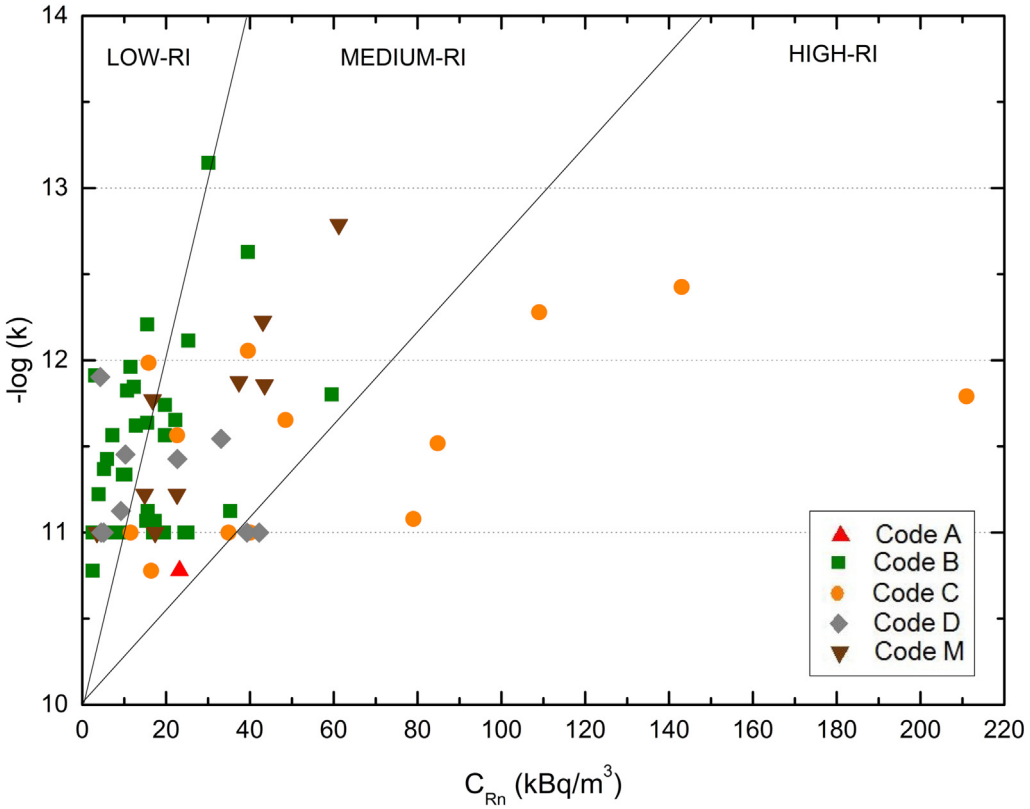

Fig. 10. Graphical representation of geogenic radon potential (GRP) divided by geological codes.

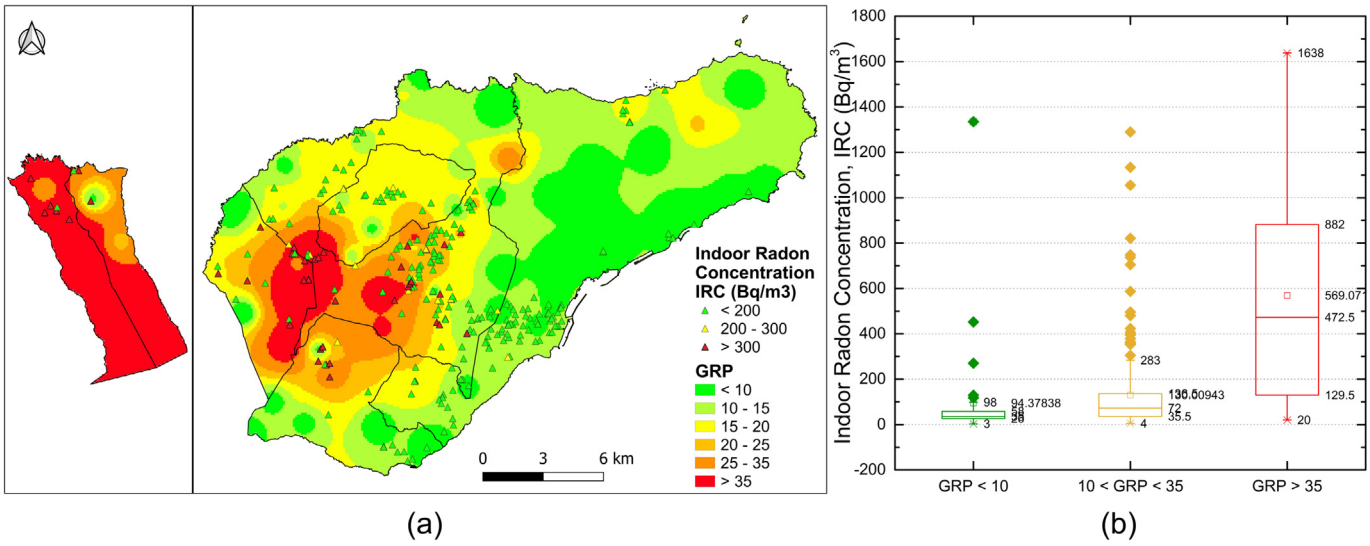

Fig. 11. Indoor radon concentration (IRC) values on geogenic radon potential (GRP) interpolation map (a), box-and-whisker plot of IRC values categorized by GRP level (b).

geometric mean of the activity concentration of ^{226}Ra in high-risk areas 91 % higher than in the low-risk area.

4) These radon risk maps were made using variables that are simpler to obtain than the direct measurement of IRC in a statistically sufficient set of dwellings in a densely populated study area. This would allow an easy implementation of the methodology in the rest of the archipelago and, in general, in volcanic territories similar to the Canary Islands.
5) This methodology allows the construction of a more detailed map of radon risk zones within the study area than the risk map currently available in the Spanish building regulations. The results of this work would

Table 10
Statistical comparison of the results of indoor radon concentration (IRC) categorized by geogenic radon potential (GRP) level.

	GRP < 10	10 < GRP < 35	GRP > 35
n	37	212	28
GM (Bq/m^3)	41.3	70.8	342.8
GSD (Bq/m^3)	3.0	3.0	3.3
UTB (Bq/m^3)	241	330	2505
P-90 (Bq/m^3)	122	305	1326

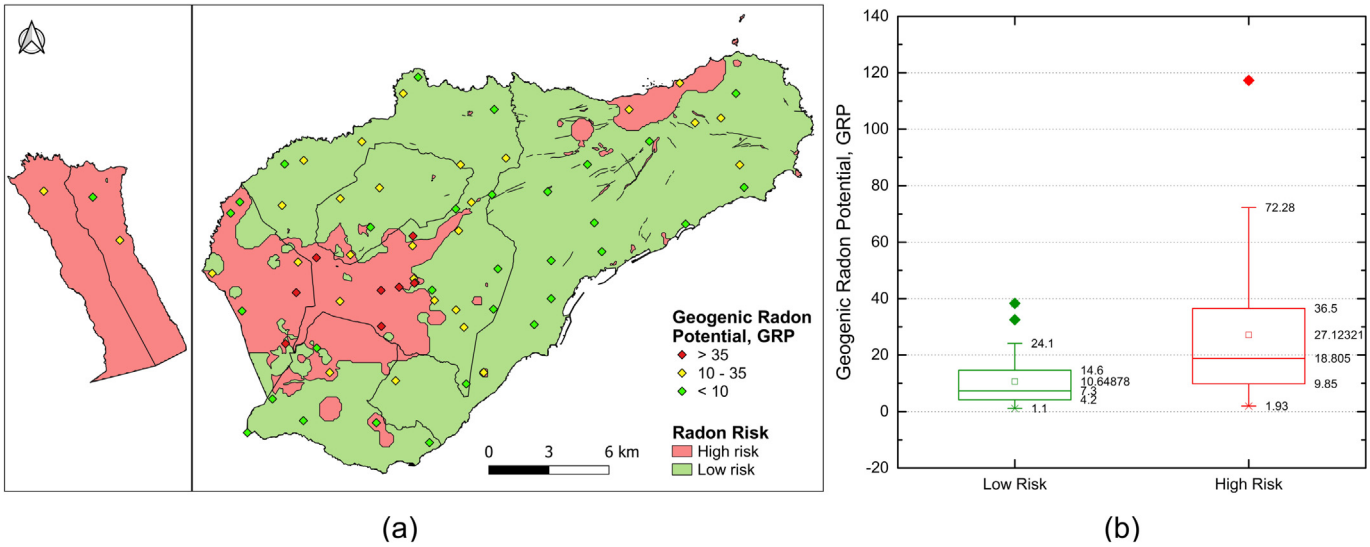

Fig. 12. Geogenic radon potential (GRP) values on combined radon risk map (a) and box-and-whisker plot of GRP values categorized by radon risk level (b).

allow certain municipalities that are currently considered as 'no-risk areas' to be reclassified as high radon risk municipalities. Conversely, other municipalities, or large parts of them, that are currently classified as 'high-risk areas' could be removed from this classification.

CRediT authorship contribution statement

Claudio Briones: Writing - Original Draft, investigation, Methodology, Visualization, Validation, Data Curation, writing - Review & Editing. **Javier Jubera:** investigation, Writing - Review & Editing, Supervision, Project administration, Methodology, Data Curation. **Héctor Alonso:** investigation, Methodology, resource, Project administration, **Jesús Olaiz:** investigation, resource, Project administration, **Juana T. Santana:** investigation, resource. **Natalia Rodríguez-Brito:** investigation, resource. **Ana del Carmen Arriola Velasquez**, investigation, Data Curation, Visualization **Neus Miquel i Armengol**, investigation, Data Curation, Visualization **Alicia Tejera:** investigation, Resource. **Pablo Martel:** investigation, resources, Data Curation. **Eduardo González-Díaz:** investigation. Formal analysis. Review & Editing, Data Curation, Supervision. **Jesús G. Rubiano:** investigation, Writing - Review & Editing, Supervision, Project administration, Methodology.

Data availability

The data that has been used is confidential.

Declaration of competing interest

The authors declare that they have no known competing financial interests or personal relationships that could have appeared to influence the work reported in this paper.

Acknowledgments

This work has been financed by Government of the Canary Islands (Consejería de obras públicas, transporte y vivienda) through the collaboration agreement with the University of Las Palmas de Gran Canaria for a "Proposal for a new zoning to predict the level of risk derived from the presence of radon concentrations inside buildings". The lithostratigraphic maps are obtained from Cartografía Digital del Mapa Geológico y Continuo de España (GEODE) supplied by Instituto Geológico y Minero de España (I.G.M.E.).

References

Alonso, H.E., 2015. El radón en suelos, rocas, materiales de construcción y aguas subterráneas de las Islas Canarias Orientales. Universidad de Las Palmas de Gran Canaria.

Alonso, H., Rubiano, J.G., Guerra, J.G., Arnedo, M.A., Tejera, A., Martel, P., 2019. Assessment of radon risk areas in the eastern Canary Islands using soil radon gas concentration and gas permeability of soils. Sci. Total Environ. 664, 449–460. https://doi.org/10.1016/j.scitotenv.2019.01.411.

Arnedo, M.A., Rubiano, J.G., Alonso, H., Tejera, A., González, A., González, J., Bolivar, J.P., 2017. Mapping natural radioactivity of soils in the eastern Canary Islands. J. Environ. Radioact. 166, 242–258. https://doi.org/10.1016/j.jenvrad.2016.07.010.

Barbosa, S., Huisman, J.A., Azevedo, E.B., 2018. Meteorological and soil surface effects in gamma radiation time series - implications for assessment of earthquake precursors. J. Environ. Radioact. 195 (September), 72–78. https://doi.org/10.1016/j.jenvrad.2018.09.022.

Briones, C., Jubera, J., Alonso, H., Olaiz, J., Santana, J.T., Rodríguez-Brito, N., Rubiano, J.G., 2021. Methodology for determination of radon prone areas combining the definition of a representative building enclosure and measurements of terrestrial gamma radiation. Sci. Total Environ. 788, 147709. https://doi.org/10.1016/j.scitotenv.2021.147709.

Carracedo, J.C., Pérez Torrado, F.J., Ancochea, E., Meco, J., Hernán, F., Cubas, C.R., Ahijado, A., 2002. Cenozoic Volcanism II: the Canary Islands. The Geological Society London.

Cinelli, G., Tondeur, F., Dehandschutter, B., 2011. Development of an indoor radon risk map of the walloon region of Belgium, integrating geological information. Environ. Earth Sci. 62 (4), 809–819. https://doi.org/10.1007/s12665-010-0568-5.

Coletti, C., Ciotoli, G., Benà, E., Brattich, E., Cinelli, G., Galgaro, A., Sassi, R., 2022. The assessment of local geological factors for the construction of a geogenic radon potential map using regression kriging. A case study from the Euganean Hills volcanic district (Italy). Sci. Total Environ. 808. https://doi.org/10.1016/j.scitotenv.2021.152064.

Ministerio de la Presidencia, R.con L.C.y M.D, 2022. Real Decreto 1029/2022, de 20 de diciembre, por el que se aprueba el Reglamento sobre protección de la salud contra los riesgos derivados de la exposición a las radiaciones ionizantes. I. Boletín Oficial Del Estado (BOE).

Darakctchieva, Z., Appleton, J.D., Rees, D.M., Adlam, K., Myers, A.H., Hodgson, S.A., Peake, L.J., 2015. Radon in Northern Ireland : indicative atlas about public health England. Retrieved fromPublic Health Engl., 14.. https://www.gov.uk/government/uploads/system/uploads/attachment_data/file/453711/PHE-CRCE-017_maps_with_place_names_.

Euratom, B.S.S., 2014. Council Directive 2013/59 EURATOM of 5 December 2013 Laying Down the Basic Safety Standards for the Protection of the Health of Workers and the General Public Against the Dangers Arising From Ionizing Radiation, and Repealing Directives 89/618. (December 1990), pp. 1–73.

Fernández de Aldecoa, J.C., 2000. Radiación natural en aire y suelos de las islas Canarias occidentales. Universidad de La Laguna.

Fernández, A., Sainz, C., Celaya, S., Quindós, L., Rábago, D., Fuente, I., 2021. A new methodology for defining radon priority areas in Spain. Int. J. Environ. Res. Public Health 18 (3), 1–16. https://doi.org/10.3390/ijerph18031352.

Font, L., 1997. Radon Generation, Entry and Accumulation Indoors. Universidad Autónoma de Barcelona.

Frutos Vázquez, B., 2009. Estudio experimental sobre la efectividad y la viabilidad de distintas soluciones constructivas para reducir la concentración de gas radón en edificaciones. Universidad Politécnica de Madrid.

García-Talavera, M., López-Acevedo, F.J., 2019. Cartografía del potencial de radón de España. Retrieved fromColección de Informes Técnicos Del Consejo de Seguridad Nuclear.

García-Talavera, M., García-Pérez, A., Rey, C., Ramos, L., 2013. Mapping radon-prone areas using γ-radiation dose rate and geological information. J. Radiol. Prot. 33 (3), 605–620. https://doi.org/10.1088/0952-4746/33/3/605.

Hernandez-Pacheco, A., Rodríguez-Losada, J.A., 1996. Geología y estructura del Arco de taganana (Tenerife, Canarias). Rev. Soc. Geol. Esp. 9 (3–4), 169–182.
Herranz, M., Jiménez, R., Navarro, E., Payeras, J., Pinilla, J.L., 2003. Procedimiento de toma de muestras para la determinación de la radiactividad en suelos: Capa superficial. Colección Inf. Técnicos 1.1 2003. Consejo de Seguridad Nuclear.
Hughes, M.B., Elío, J., Crowley, Q.G., 2022. A user's guide to radon priority areas, examples from Ireland. J. Eur. Radon Assoc., 1–12 https://doi.org/10.35815/radon.v3.7586.
I.G.M.E, 2021. Cartografía digital del Mapa Geológico y Continuo de España GEODE (Comunidad Autónoma de Canarias). Instituto Geológico y Minero de España.
Ielsch, G., Cushing, M.E., Combes, P., Cuney, M., 2010. Mapping of the geogenic radon potential in France to improve radon risk management: methodology and first application to region Bourgogne. J. Environ. Radioact. 101 (10), 813–820. https://doi.org/10.1016/j.jenvrad.2010.04.006.
López-Pérez, M., Martín-Luis, C., Hernández, F., Liger, E., Fernández-Aldecoa, J.C., Lorenzo-Salazar, J.M., Salazar-Carballo, P.A., 2021. Natural and artificial gamma-emitting radionuclides in volcanic soils of the Western Canary Islands. J. Geochem. Explor. 229 (December 2020). https://doi.org/10.1016/j.gexplo.2021.106840.
Maitre, R.W.Le, 2002. Igneous Rock. A Classification and Glossary of Terms. Recommendations of the International Union of Geological Sciences Subcommission on the Systematics of Igneous Rocks. Vol. 53. Cambridge University Press. https://doi.org/10.1017/CBO9781107415324.004.
McColl, N.P., Bradley, E.J., Gooding, T.D., Ashby, C., Astbury, J., Akinson, J., Wasson, G., 2018. UK National Radon Action Plan About Public Health England. Public Health Engalnd.
Miles, J., Appleton, J., Rees, D., Green, B.M.R., Adlam, K.A.M., Myers, A.H., 2007. . Retrieved fromIndicative Atlas of Radon in England and Wales; Report HPA-RPD-033. Public Health England , pp. 1–29.. http://www.ukradon.org/cms/assets/gfx/content/resource_2686cs3a0844cee4.pdf.
Miles, J.C.H., Appleton, J.D., Rees, D.M., Adlam, K.A.M., Scheib, C., Myers, A.H., Mccoll, N.P., 2011. Indicative Atlas of Radon in Scotland (Report HPA-CRCE-023). Public Health England, pp. 1–33 (July 2011).
Ministerio de Fomento, 2019. Documento Básico de Salubridad HS, Sección HS 6 Protección frente a la exposición de radón. Retrieved fromBol. Of. Estado 2013, 1–129.. http://www.arquitectura-tecnica.com/hit/Hit2016-2/DBHE.pdf.
Neznal, M., Neznal, M., Matolín, M., Barnet, I., Miksova, J., 2004. The New Method for Assessing the Radon Risk of Building Sites. Czech Geol. Survey Special Papers, Prague.
Pereira, A., Lamas, R., Miranda, M., Domingos, F., Neves, L., Ferreira, N., Costa, L., 2017. Estimation of the radon production rate in granite rocks and evaluation of the implications for geogenic radon potential maps: a case study in Central Portugal. J. Environ. Radioact. 166, 270–277. https://doi.org/10.1016/j.jenvrad.2016.08.022.
Pinza-Molina, C., 1998. Radón En Viviendas De Las Islas Canarias Orientales : Consecuencias De Dosimétricas. Universidad de La Laguna.
Quindós Poncela, L.S., Fernández, P.L., Gómez Arozamena, J., Sainz, C., Fernández, J.A., Suarez Mahou, E., Cascón, M.C., 2004. Natural gamma radiation map (MARNA) and indoor radon levels in Spain. Environ. Int. 29 (8), 1091–1096. https://doi.org/10.1016/S0160-4120(03)00102-8.
Robayna Duque, B.E., 2002. Radón en viviendas de las Islas Canarias occidentales. Distribución geográfica y dosimetría. Universidad de La Laguna.
Suárez-Mahou, E., Fernández-Amigot, Á., Moro, M., García-Pomar, D., Moreno, J., Lanaja, J., 2000. Proyecto Marna. Mapa de radiación gamma natural, INT-04-02. Colección Informes Técnicos Consejo de Seguridad Nuclear.
Tondeur, F., Cinelli, G., 2014. A software for indoor radon risk mapping based on geology. Nuclear Technol. Radiat. Prot. 29 (SUPPL.). https://doi.org/10.2298/NTRP140SS59T.
UNSCEAR, 1993. Sources and effects of ionazing radiation. J. Radiological Protection, Annex IV. Vol. I.
UNSCEAR, 2000. Sources and Effects of Ionizing Radiation.
World Health Organization, 2015. Manual de la OMS sobre Radón en interiores. http://www.who.int/iris/handle/10665/161913#sthash.2WvJkXnR.dpuf.